Annals of Biomedical Engineering, Vol. 14, pp. 241–256, 1986
Printed in the USA.

0090-6964/86 $3.00 + .00

MECHANICS OF THE OTOLITH ORGAN—DYNAMIC RESPONSE

J. Wallace Grant
William A. Best

Department of Engineering Science & Mechanics, Virginia Polytechnic Institute & State University, Blacksburg, Virginia

The otolith organs are the linear motion sensors of the mammalian system. As part of the vestibular system, these small organs are located in the inner ear. Mathematically modeled, they consist of an overdamped second-order system with elastic, viscous damping and mass elements. The governing equations of motion which describe the relative velocity of the mass with respect to the skull consist of a set of three coupled partial integral-differential equations. When these equations are nondimensionalized, they yield two nondimensional parameters which characterize the dynamic response of the system. These nondimensional equations are solved numerically for the relative displacement of the otolith mass for various values of the two nondimensional parameters. The solutions generated are for a step change in skull velocity. These solutions indicate that the end organ upper breakpoint frequency is at least one order of magnitude higher than previously measured experimental values determined by first-order neuron recordings.

Keywords—*Otolith model, Numeric solution, Frequency response.*

INTRODUCTION

The mammalian inner ear consists of two distinct sections, the auditory portion responsible for the sense of hearing and the nonauditory or vestibular section whose primary function is to sense skull motion and gravity. The motion and gravity information is used by the central nervous system for control of posture and visual image fixation. Visual image fixation is accomplished by compensatory eye movement in a direction opposite to that of the skull. One's sensation of motion is also derived from these end organ sensors, and they are used in coordination of muscular activity during periods of body motion. The vestibular organs can be further subdivided into the semicircular canals which response to changes in angular acceleration and the otolith organs which sense changes in linear velocity as well as responding to gravity.

Acknowledgement—This study was supported in part by a Research Initiation Grant From the Engineering Foundation, Grant No. RI-A-82-9.

Address correspondence to J. Wallace Grant, Engineering Science & Mechanics Department, Virginia Polytechnic Institute and State University, Blacksburg, VA 24061.

The four otolith organs, two in each ear, are contained in fluid-filled chambers that are situated in the bony labyrinth, a hollowed-out section of the temporal bone of the skull. The otoliths are flat plane structures, and the two planes of each organ in a single ear are mutually perpendicular to each other. These organs are also directionally sensitive in the plane of the organ and do not have the capability of sensing motion normal to their plane. The perpendicularity of the two organ planes combined with their directional sensitivity allows the otolith system to effectively sense motion and gravity in each of three mutually perpendicular planes.

The composition of each otolith consists of three discrete parts: the otoconial membrane, the cupular membrane and the sensory hair cell base. This composition is shown schematically in Fig. 1. The otoconial membrane is an aggregation of stone-shaped calcium carbonate crystals (otoconia) embedded in a gelatinous membrane. This gelatinous membrane is composed of a mucopolysaccharide material which has a density of 1.0 gm/cm^3 (12). The otoconial crystals are less than 10 μm in diameter (1) and have a density of 2.71 gm/cm^3 (2). To date, there has been no measurement of what percentage of these crystals is contained in the total otoconial membrane volume: thus the density of the membrane is undetermined. In our model this is a parameter necessary for the accurate determination of the dynamic response of the otolith system. In addition to the density, the thickness of this membrane has not yet been determined for humans. However, this thickness has been measured and is reported to be 15 μm for the squirrel monkey (3).

The otoconial membrane's top surface is in contact with a fluid that partially fills the inner ear called endolymph [density $\rho = 1.0$ gm/cm^3, and viscosity $\mu = 0.85$ centipoise (4)]. The otoconial membrane's lower surface is attached to a highly deformable elastic gelatinous material, the cupular membrane, which is a continuation of the gelatinous material of the otoconial membrane. This cupular membrane material is attached to sensory tissue which is in turn rigidly attached to the temporal bone of the skull.

The sensory tissue consists of hair cells which are embedded in connective tissue. Protruding from the hair cells at the cupular membrane interface and extending into the cupular membrane are discrete bundles of sensory hairs. When the skull is

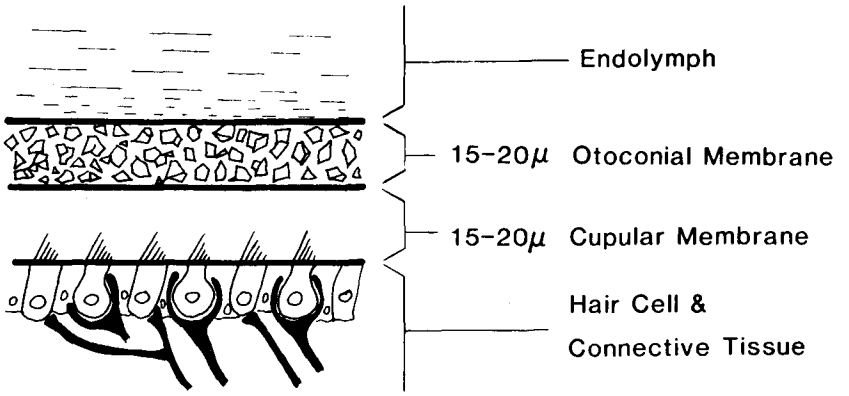

FIGURE 1. Schematic composition of the otolith organs showing the discrete parts: Endolymph, Otoconial Membrane, Cupular Membrane and Sensory Base [after Igarashi (3)].

accelerated the otoconial membrane tends to lag behind the sensory base due to its inertia. This relative motion of the otoconial membrane with respect to the sensory cell base causes a shearing deformation of the cupular membrane. The resultant deformation of the cupular membrane is sensed by the hair cells, transduced into trains of nervous action potentials, and sent to the central nervous system via the vestibular nerve. Gravity can also cause a similar shearing deformation of the cupular membrane which also changes the nervous firing rate.

The otolith organs are a second-order mechanical system with mass, viscous damping and an elastic element. The mass element consists of the otoconial membrane: the viscous damping element arises from the viscous shear between the otoconial membrane and the fluid endolymph, and the elastic element comes from shear deformation of the cupular membrane. This system is highly overdamped, and evidence of this behavior was first offered by DeVries (5), who used x-ray methods to measure the movements of the otoconial membrane in fish. This over critically damped behavior has also been demonstrated using human subjects (6).

An overdamped second-order seismic system of this type is a velocity sensor and the mass displacement (in the otolith system this is the otoconial membrane displacement measured with respect to the skull) is proportional to the velocity of the base or frame to which the second-order system is attached. This relationship remains valid over a certain dynamic range or "bandwidth" of system input frequencies. Thus the system dynamics can be described by the system gain and two breakpoint frequencies which determine the system bandwidth. Experimental efforts to evaluate the system dynamics have centered around measurement of the system breakpoint frequencies (6,9,13). These measurements were made utilizing subjective sensation, ocular torsion and first order neuron recordings. All of these experimental determinations included biologic system elements other than just the end organ sensor itself, the otolith. These other system elements include hair cell transduction, neural transmission, neural computation, muscle contractions and eye dynamics, to name a few. These other system elements tend to modify the actual otolith dynamic response such that the experimental results represent the entire system and not the end organ by itself. One method of evaluating the dynamics of the otolith sensor without the other system elements involved is to use a theoretical dynamic analysis of the end organ.

The only previous theoretical effort to quantitatively describe the system dynamics of the otolith organs is that of the author's (7). The objectives of the present work were to extend this effort and draw some conclusions about the dynamics of the system. Specifically, the governing equations of motion have been written from a continuum mechanics or distributed parameter approach instead of a lumped parameter system. These equations are solved using numeric methods, and conclusions about the system dynamics are extracted from the results. A value for the upper breakpoint frequency of the human otolith is determined from these results, and this value is compared with the experimentally measured values. There is an order of magnitude difference in the experimental and theoretical values. This discrepancy is discussed at the conclusion of this paper.

GOVERNING EQUATIONS OF MOTION

The governing equations of motion for the otolith organs have been derived by Grant *et al.* (7) and are repeated here for continuity and clarity. In the derivation

of these equations the otoliths were treated as flat planes with infinite extent. This infinite extent assumption is justified on the basis that the end effects can be shown to be negligible due to the small thickness of the organ compared to its surface area. The end area, where normal pressure forces may act, is approximately 100 times smaller than the flat plane surface area. In addition, the pressure forces which act on the end area are an order of magnitude smaller than the viscous shear forces acting on the upper plane surface. The pressure-induced forces acting on the end area are thus three orders of magnitude smaller than the viscous surface forces.

Figure 2 illustrates a two-dimensional, cross-sectional view of the human otolith geometry used in this study. For this analysis it has been partitioned into three separate, distinct parts: (1) the fluid (endolymph), (2) the rigid plate (otoconial membrane) and (3) the elastic deformable base (cupular membrane). Figure 3 illustrates the free-body diagram of each element with associated forces. It is important to note that the fluid element is coupled to the plate element by τ_f (fluid shear stress) and the plate element is coupled to the elastic element by τ_e (elastic shear stress).

The governing equations of motion for the otolith system determined from these free-body diagrams are

For the *Fluid Endolymph:*

$$\rho_f\left(\frac{\partial u}{\partial t}\right) = \mu\left(\frac{\partial^2 u}{\partial y^2}\right) , \tag{1}$$

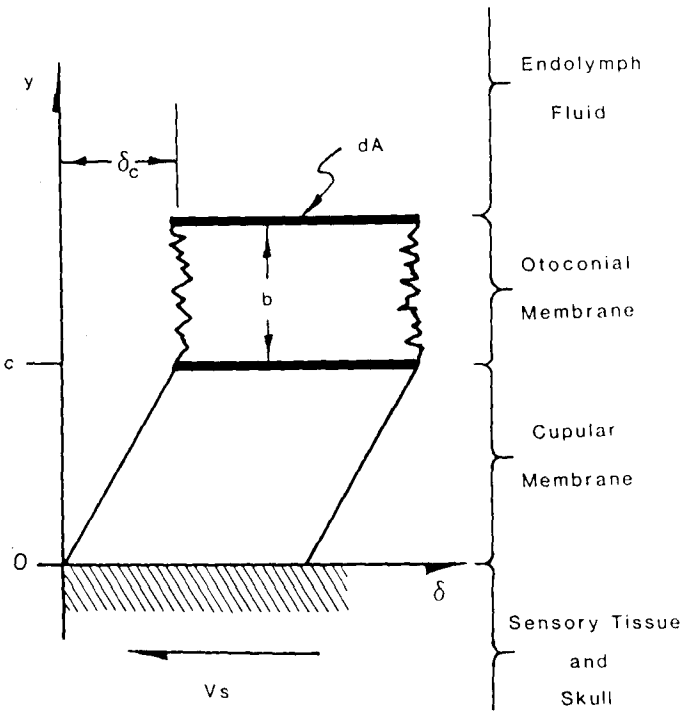

FIGURE 2. Two-dimensional cross-section of the otolith organ illustrating geometry used in this study.

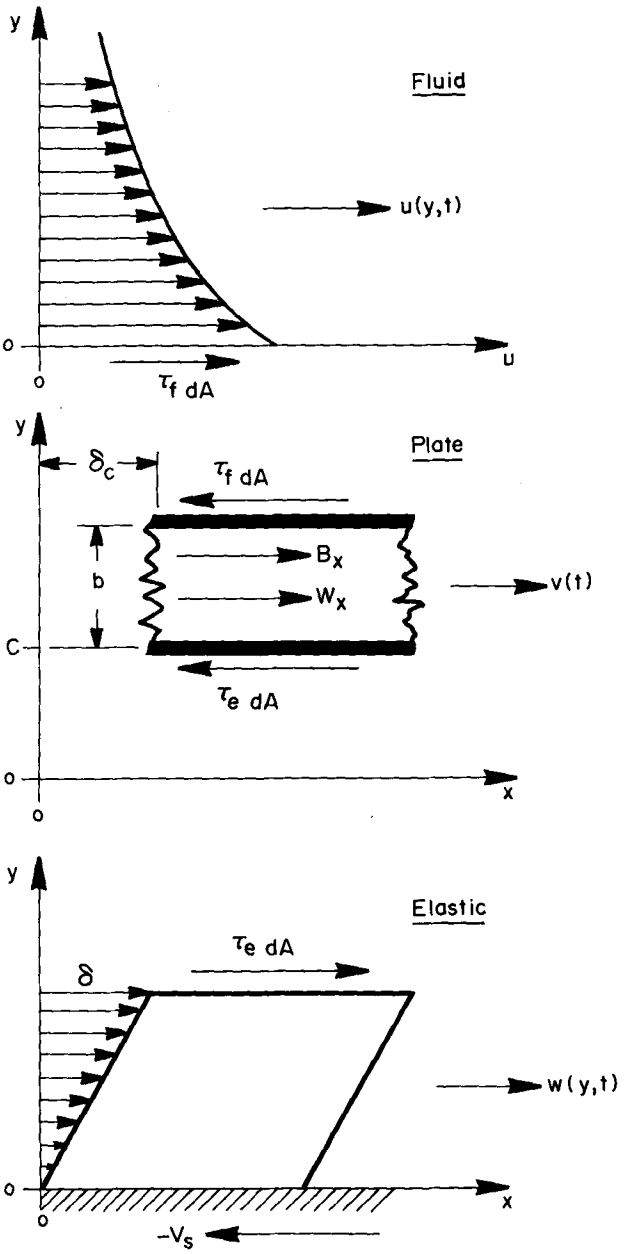

FIGURE 3. Three elemental parts of the otolith showing free-body diagrams of each element.

with the following boundary conditions:

$$u(0,t) = v(t) \text{ and } u(\infty,t) = 0 \ , \tag{1a}$$

where $u(y,t)$ is the velocity of the endolymph fluid in the x-direction measured with respect to the skull, ρ_f is the density of the endolymph fluid, μ is the endolymph vis-

cosity, and $v(t)$ is the velocity of the otoconial membrane (plate) in the x-direction measured with respect to the skull.

For the *Otoconial Membrane:*

$$-\frac{1}{2}\left(\frac{E}{1+\nu}\right)\int_0^t \left(\frac{\partial w}{\partial y}\bigg|_c\right) \mathrm{d}t + \mu\left(\frac{\partial u}{\partial y}\bigg|_0\right) = \rho_0 b\left(\frac{\partial v}{\partial t}\right) + (\rho_0 - \rho_f)b\left[\frac{\partial V_S}{\partial t} - g_x\right] , \quad (2)$$

where w is the velocity of the cupular membrane in the x direction measured with respect to the skull, V_s is the velocity of the skull in the x-direction measured with respect to an inertial reference frame, E is Young's modulus of the cupular membrane material, ν is Poisson's ratio of the cupular membrane material, ρ_0 is the density of the otoconial membrane, g_x is the component of the gravity vector acting in the x-direction, b is the thickness of the otoconial membrane and c is the thickness of the cupular membrane.

For the *Elastic Cupular Membrane:*

$$\rho_f\left(\frac{\partial w}{\partial t}\right) = \frac{1}{2}\left(\frac{E}{1+\nu}\right)\int_0^t \left(\frac{\partial^2 w}{\partial y^2}\right) \mathrm{d}t , \quad (3)$$

with boundary conditions

$$w(c,t) = v(t) \text{ and } w(0,t) = 0 . \quad (3a)$$

The two thicknesses b and c are approximately equal to one another, and we will assume that $b = c$ in the analysis.

These equations may now be nondimensionalized by substitution of the following nondimensionalized variables indicated by bars:

$$\bar{y} = \frac{y}{b} , \quad \bar{t} = \frac{\mu}{\rho_0 b^2} t , \quad \bar{u} = \frac{u}{V} , \quad \bar{w} = \frac{u}{V} , \quad \bar{v} = \frac{v}{V} , \quad \bar{V}_s = \frac{V_s}{V} , \quad (4)$$

where V is some characteristic velocity in the problem, e.g. magnitude of a step change of skull velocity. This substitution leads to three nondimensional governing equations for the dynamic behavior of the otolith organs:

$$R\,\frac{\partial \bar{u}}{\partial t} = \frac{\partial^2 \bar{u}}{\partial \bar{y}^2} , \quad (5)$$

$$\bar{u}(0,\bar{t}) = \bar{v}(\bar{t}) \text{ and } \bar{u}(\infty,\bar{t}) = 0 , \quad (5a)$$

$$\frac{\partial \bar{v}}{\partial t} + (1-R)\left[\frac{\partial \bar{V}_s}{\partial \bar{t}} - \bar{g}_x\right] = \frac{\partial \bar{u}}{\partial \bar{y}}\bigg|_0 - \epsilon\int_0^{\bar{t}} \left(\frac{\partial \bar{w}}{\partial y}\bigg|_1\right) \mathrm{d}\bar{t} , \quad (6)$$

$$R\left(\frac{\partial \bar{w}}{\partial \bar{t}}\right) = \epsilon\int_0^t \left(\frac{\partial^2 \bar{w}}{\partial \bar{y}^2}\right) \mathrm{d}\bar{t} , \quad (7)$$

$$\bar{w}(1,\bar{t}) = \bar{v}(\bar{t}) \text{ and } \bar{w}(0,\bar{t}) = 0 , \quad (7a)$$

in which the following naturally occurring nondimensional parameters were utilized:

$$R = \frac{\rho_f}{\rho_0} \text{ and } \epsilon = \frac{1}{2}\left(\frac{E}{1+\nu}\right)\left(\frac{b^2}{\mu^2}\right)\rho_0 \ , \tag{8}$$

and the nondimensional gravity $\bar{g}_x$ is defined in the nomenclature section at the end of this article. This set of coupled equations is parabolic and can display underdamped oscillatory behavior: however, we are interested only in the overdamped solutions. This concludes the review of the previously derived governing equations (7), and the work from this point on represents new material.

The main objective of this work was to determine solutions to this set of nondimensional governing equations for the condition of a step change in skull velocity [$V_s = V\delta(t)$, where $\delta(t)$ is the unit step function] and with $\bar{g}_x = 0$, for various values of the dimensionless parameters R and ϵ. The numeric value of ϵ is small, when calculated from available data it lies in the range of $\epsilon \leq 0.02$. Consequently, an analytic solution for $\epsilon = 0$ will aid the understanding of the system dynamics and is easily obtained by Laplace transform methods. This solution for the velocity of the otoconial membrane plate is

$$\bar{v}(\bar{t}) = (1 - R)e^{R\bar{t}} \ \text{Erfc}(\sqrt{R\bar{t}}) \ , \tag{9}$$

where Erf*c* is the complementary error function. The nondimensional displacement of the otoconial membrane plate can be found by integration of Eq. 9, and the conversion to real spatial units of displacement is given in the nomenclature section.

In order to obtain solutions for cases other than when $\epsilon = 0$, numeric integration of the governing equations is necessary. These numeric approximations were carried out using two different techniques. The first solution utilized a finite fluid boundary at a sufficient distance to introduce negligible error, instead of the boundary condition at infinity. The second method involved a transformation of the governing equations whereby the infinite fluid half-space was transformed into a strip of finite width.

In both cases finite difference techniques were utilized for the numeric solution. This method was chosen in order to accommodate the integral term in the governing equations. The use of Runge-Kutta integration subroutines as a method of solution was considered, but they do not easily lend themselves to equations which contain integral terms and were eliminated from further consideration.

Solution I: Infinite Boundary Condition

The finite difference solution to any differential equation requires that the spatial coordinate be divided into discrete points. The boundary condition where the fluid velocity at infinity equals zero introduces the first difficulty in the numeric solution, since the infinite spatial domain cannot be divided into a finite number of discrete points. This can be handled by replacing the boundary condition, $u(\infty, t) = 0$ by $u(x_f, t) = 0$, where x_f was chosen at a sufficient finite distance so as not to contaminate the long time solution.

The validity and accuracy of this method was confirmed by comparison of the numeric solution with the analytic solution for $\epsilon = 0$. For this comparison, the error between the numeric and analytic solutions for fluid velocities, and otoconial mem-

brane displacements was significantly less than 1% for all times considered in this work.

The Crank-Nicolson finite difference scheme was used in the formulation of difference equations and a stability analysis showed these difference equations to be stable for all values of $\Delta t/(\Delta y)^2 \geq 0$, where Δt is the time step increment, and Δy is the spatial increment.

The interface between the fluid and otoconial membrane introduces a Neumann boundary condition where the fluids equation (Eq. 5) and the otoconial membrane plate equation (Eq. 6) must hold at $\bar{y} = 0$. This situation was handled by the standard method of introducing a fictitious point in both equations and algebraic substitution to eliminate this fictitious point. Thus the difference equation at $\bar{y} = 0$ incorporates both the fluid and plate equations. Since the otoconial membrane plate equation also incorporates the elastic integral term, the entire problem is contained in the difference equation at $\bar{y} = 0$ and the fluid equation for all points beyond this boundary.

The integral term must now be represented in the discrete notation for finite differencing. Assuming that the cupular membrane is deformed in simple shear, the velocity slope at the boundary ($\bar{y} = 1$) may be represented as

$$\left.\frac{\partial \bar{w}}{\partial \bar{y}}\right|_{\bar{y}=1} = \frac{[\bar{w}(1,\bar{t}) - \bar{w}(0,\bar{t})]}{[1-0]} \quad , \tag{10}$$

where the velocity $\bar{w}(0,\bar{t}) = 0$. The integral can be replaced by a discrete sum utilizing the trapezoidal rule of numerical integration.

Representing the discrete time steps by n, where n denotes the present time, and $n+1$ denotes the new time equal to $t + \Delta t$, and summing over the total number of time steps an approximate expression for the integral term becomes

$$\epsilon \int_0^{\bar{t}} \left.\frac{\partial \bar{w}}{\partial \bar{y}}\right|_{\bar{y}=1} \mathrm{d}\bar{t} \simeq \epsilon \left[\left\{ \sum_1^n (\bar{w}_{1,n})\ \Delta t \right\} + (\bar{w}_{1,n+1})\ \Delta t \right] \quad , \tag{11}$$

where $\bar{w}_{1,n}$ is the velocity $\bar{w}(1,t)$ and $\bar{w}_{1,n+1}$ is the velocity $\bar{w}(1,\ t+\Delta t)$.

The value of $w_{1,n+1}$ can be grouped with the unknown velocities at the $n+1$ time step. This grouping retains the linear nature of the governing equations.

The expression for the integral term was incorporated into the set of finite difference equations previously discussed. This set of equations forms a tridiagonal coefficient matrix which can subsequently be solved by application of the Thomas algorithm (15). The deflection of the otoconial membrane can then be calculated by numeric integration of the resulting velocity $\bar{v}$.

Solution II: Transformation

The previous solution assumed a finite spatial point x_f where the velocity was arbitrarily set to zero $[u(\infty,t) = 0 \simeq u(x_f,t)]$. In order to eliminate the boundary condition at infinity, the following transformation was imposed on the original set of governing equations (8). If we let

$$\bar{Y} = 1 - \mathrm{e}^{-\bar{y}} \quad , \tag{12}$$

it is clear that the boundaries are changed as follows:

$$\bar{y} = 0 \rightarrow \bar{Y} = 0 \ ,$$

$$\bar{y} = \infty \rightarrow \bar{Y} = 1 \ , \tag{13}$$

thus transforming the original infinite half-space domain from $0 \rightarrow \infty$ to a new domain, a strip, from $0 \rightarrow 1$. This transformation changes the original governing equations as follows for the fluid and plate equations:

$$R \frac{\partial \bar{u}}{\partial \bar{t}} = (1 - \bar{Y})^2 \frac{\partial^2 \bar{u}}{\partial \bar{Y}^2} - (1 - \bar{Y}) \frac{\partial \bar{u}}{\partial \bar{Y}} \ , \tag{14}$$

$$\frac{\partial \bar{u}}{\partial \bar{t}} + (1 - R) \left[\frac{\partial \bar{V}_s}{\partial \bar{t}} \right] = (1 - \bar{Y}) \frac{\partial \bar{u}}{\partial \bar{Y}} - \epsilon \int_0^{\bar{t}} (1 - \bar{Y}) \frac{\partial \bar{u}}{\partial \bar{Y}} \, d\bar{t} \ , \tag{15}$$

where the cupular membrane equation is no longer needed due to the representation of the integral elastic term by Eq. 10.

Because of the inherent numeric instabilities in the transformed equations, the use of an implicit finite difference scheme was necessary in order to solve this set of equations. As discussed earlier, the fluids equation is coupled to the plate equation introducing the Neumann boundary condition which is again handled by the fictitious point method. The integral term is also handled exactly as before.

Comparison of these results with the analytic solution for velocities and displacements with $\epsilon = 0$ indicate an error significantly less than 1% for all times considered in this work. Further comparisons of these results with the previous solution (infinite boundary) show an exact match of velocities and displacements out to and usually beyond the fourth significant figure. However, the previous infinite half-space model required significantly less computer time than did the present transformed model.

RESULTS AND CONCLUSIONS

The overall behavior of the governing equations for various values of ϵ and constant R is represented in Fig. 4. The nondimensional parameter ϵ is a measure of the elastic response of the cupular membrane, and it is clear from these curves that as ϵ increases the maximum otoconial membrane displacement decreases, as does the time necessary to reach this maximum displacement. As ϵ continues to increase, the dynamic response of the system becomes less overdamped until the point of critical damping is passed and oscillation occurs. Oscillatory response was not considered as a viable solution, since the otolith system is over critically damped. For other values of R, overall behavior is similar to that shown in Fig. 4.

Figure 5 depicts a family of curves for various values of R and constant ϵ. The time to reach maximum displacement is approximately the same for any physiologic value of R. Similar behavior can be seen for any value of ϵ utilized in this study. As R increases (decreasing ρ_0), the maximum displacement of the otoconial membrane decreases.

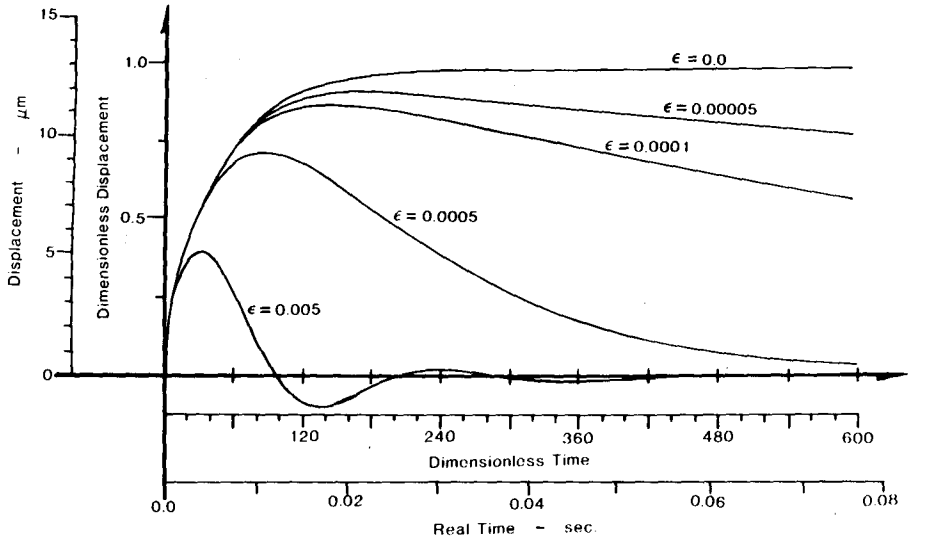

FIGURE 4. Displacement of the otoconal membrane measured with respect to the skull versus time for various values of ϵ and constant R ($R = 0.91$, $\rho_0 = 1.1$). Real time and displacement scales are shown for the following physical values: $b = 10$ μm, $\rho_0 = 1.1$ gm/cm^3, $\mu = 0.85$ centipoise, and $V = 10$ cm/s.

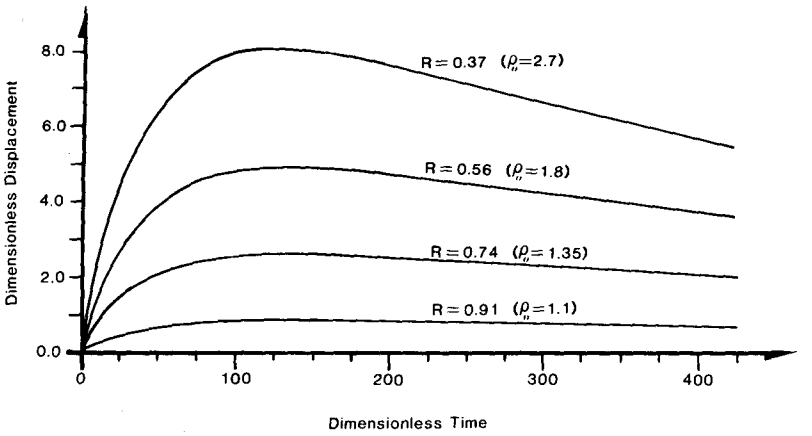

FIGURE 5. Dimensionless displacement of the otoconial membrane versus dimensionless time for various values of R and constant ϵ ($\epsilon = 0.000\,05$).

Figure 6 illustrates dimensionless velocity profiles at various dimensionless times. The velocities become negative after a finite period of time due to the presence of the elastic element (cupular membrane) which drives the otoconial membrane back to its equilibrium position. As can be seen, as long as the velocities are everywhere positive the velocity profiles propagate outward with increasing time.

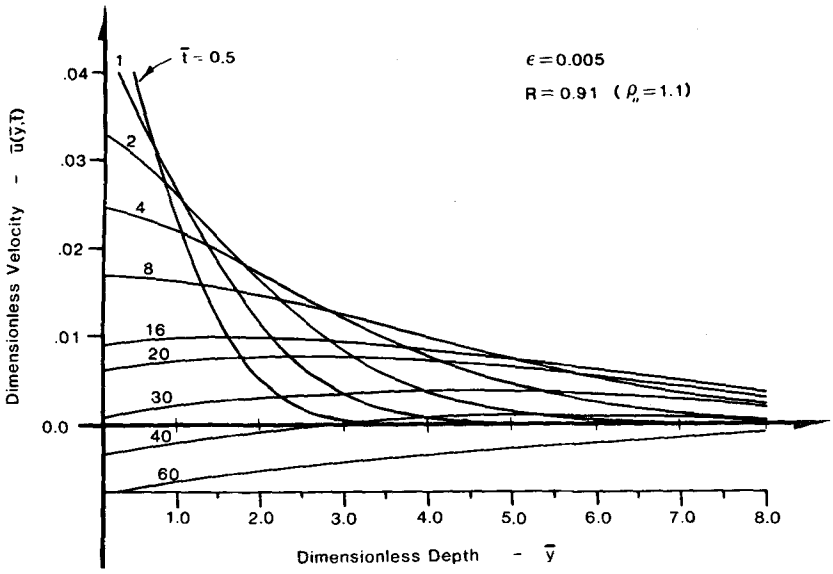

FIGURE 6. Velocity profiles (dimensionless velocity of the otoconial membrane versus dimensionless depth of the endolymph fluid) for various dimensionless times ($\epsilon = 0.005$, $\rho_0 = 1.1$).

In order to establish a range of values of R and ϵ for the human otolith system, it was necessary to consider the histologic composition of the otoconial membrane and its maximum displacement. From a composition viewpoint, the otoconial membrane is composed of crystals embedded in cupular material. Since the membrane is not comprised of 100% crystals, the density of the otoconial membrane can conceivably vary between 1.0 gm/cm^3, the density of the cupular material (12), and 2.71 gm/cm^3, the density of the crystals (1). A photomicrograph (3) shows the membrane to be less than half crystals, so that a value of ρ_0 ranging between 1.8 and 1.0 seems reasonable for the otoconial membrane density.

By considering the maximum displacement of the otoconial membrane this range of densities can be narrowed further. A value of $\epsilon \leq 0.000\,05$ was selected to best represent the otolith system, since that value produces no overshoot and results in long return times to equilibrium. With $\epsilon = 0.000\,05$, two maximum nondimensional displacements for $\rho_0 = 1.35$ and 1.10 were selected and converted to dimensional displacements. For this conversion the otoconial membrane thickness was chosen to be 10 μm, the endolymph viscosity was $\mu = 0.85$ centipoise, and the step change in skull velocity was 10 cm/s. This produced values of the otoconial membrane displacement $\delta = 42$ μm for $\rho_0 = 1.35$ and $\delta = 11$ μm for $\rho_0 = 1.10$. In order for this displacement to be in the same range as the cupular membrane thickness the density must be in the range $\rho_0 = 1.10$.

Experimental results in this field have all assumed lumped parameter models for analysis of collected data. In order to compare the results of this distributed parameter model with experimental results we must first establish common grounds for comparison. This comparison will be carried out utilizing a linear lumped parameter model which can be used to describe the overdamped displacement dynamics of

the otoconial membrane measured with respect to the skull (11). With such a lumped parameter model, the solution for a step change in skull velocity indicates that the initial displacement of the otoconial membrane can be described by an exponential. This exponential displacement predicted by the lumped parameter model can be compared to the distributed parameter model considered here. A value for a time constant can be determined which approximates the numeric solutions of this work. With this time constant determined, comparison with other experimentally determined time constants can be made. It should be noted that the reciprocal of this time constant represents the upper breakpoint frequency of the system. The evaluation of this time constant is carried out in the next paragraph with comparisons and discussions in the following paragraphs.

The initial displacement phase of the otoconial membrane described by a lumped parameter model is given by

$$\delta(t) = \delta_{\max}(1 - e^{-t/\tau}) \ , \tag{16}$$

where $\delta(t)$ is the displacement of the otoconial membrane measured with respect to the skull at time t, $\delta_{\max}$ is the maximum displacement, and τ is the time constant. Referring to Fig. 5, it can be determined that for $\rho_0 = 1.10$, the maximum displacement of the otoconial membrane is 0.88 which occurs at a dimensionless time of 174 (0.0113 real-time seconds). With $t/\tau = 5$, since at 5 time constants the solution has reached 99.4% of its maximum, $\tau = 174/5 = 34.8$ dimensionless time units. This converts to a real time of 0.002 25 sec which yields an upper breakpoint frequency of 440 rad/sec. Figure 7 compares Eq. 16 for a lumped parameter model to that of our distributed parameter model. The close agreement of the two curves, for the initial displacement phase, indicates that a lumped parameter model does approximate the distributed parameter model well.

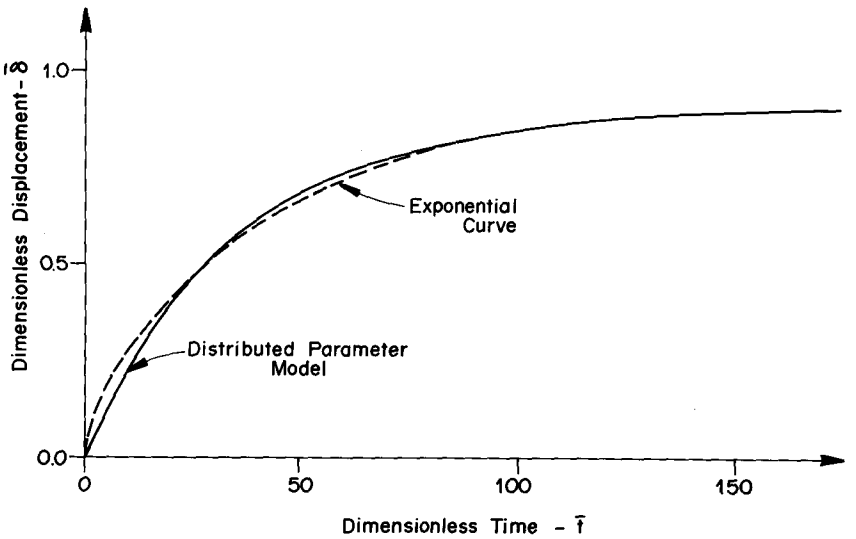

FIGURE 7. Comparison of exponential curves fit to numeric model.

The above approximation of the breakpoint frequency is our best estimate of this value based upon available evidence and current data. It should be noted that if one determines the lower limit of this frequency using current anatomical and physical data it would be approximately 200 rad/sec. The theoretical analysis of the work indicates that the breakpoint frequency must lie above 200 rad/sec. It should also be noted that lumped parameter analysis has been unable to predict this upper breakpoint frequency due to the inability to theoretically evaluate the lumped parameter coefficients (11). The distributed parameter model considered here is the first theoretical attempt to evaluate this upper breakpoint frequency.

If one compares the upper breakpoint frequency of 440 rad/sec determined from the present model to that obtained from ocular and perceptual data of 1.5 rad/sec (6,9), and first-order neuron recordings of 62.5 rad/sec (13), it is obvious that the analytical model differs quite substantially. This is not to say that either the model, or the experimental evidence is incorrect, but rather we believe that they represent upper breakpoint frequencies measured and predicted at different locations in the overall system.

The experimentally determined values derived from perceptual and occular data use methods which involve monitoring occular torsional displacement response or subjective sensation to specific motion stimuli (6,9). Since these experimental measurements included other human system elements, the most dominant being the dynamics of the eye muscles and eye, the measured time constant reflects the dynamics of these slower system elements. The end organ transducer, the otolith, should be the fastest overall system component for good dynamic system response. In addition, if one examines the dynamics of eye motion as well as muscle dynamics, it is not hard to conceive that these two elements have a response in the range of the experimentally determined values. Again, good system design would require this element to be the slowest in the system.

The first-order neuron data was measured from vestibular nerves leading directly from the otoliths (13). The skull was then given a prescribed motion and the resultant nerve signal recorded. These recordings still contained other system elements including nervous signal transmission delays, sensory hair cell transduction and hair cell adaptation. Their signals are an order of magnitude faster than the perceptual and reflex data indicating an increased system dynamic response. The end organ transducer, the otolith, should again be the fastest system element, and indeed the theoretical analysis of this work indicates that there is an additional order of magnitude increase in the frequency response of this mechanical end organ transducer. It is interesting to note that the system dynamic response increases by an order of magnitude at succeeding levels as one approaches the transducer. This system design probably reflects the evolutionary requirements to match the system to the dynamic needs of the animal.

DISCUSSION

The preceding analysis is the first attempt to quantify the dynamic response of the otoliths from a theoretical analysis and draw specific conclusions regarding their response. However, in order to accomplish this, several assumptions have been made that will need refinement in future research. The supposition concerning simple shear deformation of the cupular membrane may be incorrect. This tissue may show non-

linear soft tissue behavior; however, this is not likely, since it does not contain any collagen or collagenous structure. Although no definitive evidence has yet been determined, the cupular material may have viscoelastic properties and not the hypothesized pure elastic behavior used in this analysis. If this were true, more damping would be introduced into the system, and the analysis here would be changed significantly. All available evidence indicates that the model considered here needs more viscous damping. This can be confirmed by considering maximal otoconial membrane displacement and comparing the experimentally measured lower breakpoint frequency with the long-time results of this work. A viscoelastic cupular material has been considered by DeVries (5) where he placed all the system damping in this element and ignored the contribution of the endolymph.

All anatomical dimensions and material properties used in the model, (ρ_0, E, ν, thickness of otoconial membrane and cupular membrane, smoothness of the otoconial membrane surface, etc.) were either extrapolated from animal studies or surmised. In order to arrive at a more precise and accurate model, experimental studies are necessary to determine exact values for these physical constants and dimensions.

Even with these flaws we feel that this model does depict the behavior of the otolith system better than any experimentally measured dynamic response. The inclusion of other slower natural system elements in these experimentally measured values reflects the slower element dynamics and not the otoliths. If the breakpoint frequency analysis carried out here was performed using the entire range of the physiologic parameters outlined earlier, our model still predicts a breakpoint frequency that is two orders of magnitude greater than occular and perceptual experimental data and one order of magnitude greater than first-order neuron data. This analysis indicates that these experimental methods are not measuring true otolith function but rather reflect the slower system elements dynamics. From this theoretical analysis it is apparent that the otolith response is much faster than the experimentally determined values.

It should be noted that a similar discrepancy between experimentally measured and theoretically determined upper breakpoint frequency occurred with the semicircular canals (10,11,14). The experimentally determined values were two orders of magnitude less than the theoretical upper breakpoint frequency. The generally accepted values in use today are those determined by theoretical analysis. In this situation it is generally agreed that the experimental values measure slower system element response instead of the canals themselves.

It should be emphasized that there is significantly more information available about the semicircular canal system relative to that available from the otolith sensory apparatus. This information is available at all levels of semicircular canal function, from end organ biomechanics to central nervous system utilization of canal signals. The biomechanics modeling effort in this work is the first with any quantitative content and can be added to the total otolith system information as a step in accumulating a similar amount of understanding equivalent to that of the canals.

While it is obvious that further refinements to this model are necessary in order to accurately quantify the function of the otoliths, this research is necessary not only for the effective overall understanding of motion sensing and motion sickness mechanisms, but also for the basic comprehension of human reflex pathways, and potential diagnostic and prosthetic applications.

REFERENCES

1. Carlstrom, D. Crystallographic studies of the vertebrate otoliths. *Biol. Bull.* 125:441–463, 1963.
2. Carlstrom, D., H. Engstrom and S. Hjorth. Electron microscope and X-ray diffraction studies of statoconia. *Laryngoscope* 63:1052–1057, 1953.
3. Igarashi, M. Dimensional study of the vestibular end organ apparatus. Second symposium on the role of vestibular organs in space exploration, NASA, 1966, pp. SP-115.
4. Steer, R.W. The influence of angular and linear acceleration and thermal stimulation on the human semicircular canal. Sc.D. thesis, MIT, 1967.
5. DeVries, H.L. Mechanics of the labyrinth otoliths. *Acta Oto-Laryng.* 38:262–273, 1950.
6. Young, L.R. and J.L. Miery. A revised dynamic otolithic model. *Aerospace Med.* 39:606–608, 1968.
7. Grant, J.W., W.A. Best and R. LoNigro. Governing equations of motion for the otolith organs and their response to a step change in velocity of the skull. *J. Biomech. Engng* 106:302–308, 1984.
8. Becker *et al.* Heat diffusion with time dependent convective boundary conditions. *Numer. Meth. Engng* 19:1871–1880, 1983.
9. Young. L.R. *et al.* Occular torsion on earth and in weightlessness. *Ann. NY Acad. Sci.* 374:80–91, 1981.
10. Mayne, R. The constants of the semicircular canal differential equation. Goodyear Aerospace Corp., Report GERA-1083, 1965.
11. Wilson, V.J. and G.M. Jones. *Mammalian Vestibular Physiology.* New York: Plenum, 1979.
12. Money, K.E. *et al.* Physical properties of fluids and structures of vestibular apparatus of the pigeon. *Am. J. Physiol.* 220:140, 1971.
13. Fernandez, C. and J.M. Goldberg. Physiology of peripheral neurons innervating otolith organs of the squirrel monkey. III. response dynamics. *J. Neurophysiol.* 39:996, 1976.
14. Oman, C.M. and L.R. Young. The physiological range of pressure difference and cupular deflection in the human semicircular canal. *Acta Oto-Laryng.* 74:324, 1972.
15. von Rosenberg, Dale U. *Methods for the Numerical Solution of Partial Differential Equations.* New York: Elsevier, 1969.

NOMENCLATURE

x = coordinate direction in the plane of the otoconial membrane
y = coordinate direction perpendicular to the otoconial membrane
t = time
$u(y,t)$ = velocity of the endolymph fluid in the x-direction with respect to the skull
$v(t)$ = velocity of the otoconial membrane in the x-direction with respect to the skull
$w(y,t)$ = velocity of the of the cupular membrane in the x-direction with respect to the skull
V_s = velocity of the skull in the x-direction with respect to an inertial reference frame
$\delta(y,t)$ = displacement of the cupular membrane in the x-direction with respect to the skull
$\delta_c(t)$ = displacement of the otoconial membrane in the x-direction with respect to the skull
ρ_0 = density of the otoconial membrane
ρ_f = density of the endolymph fluid
μ = viscosity of the endolymph fluid
g_x = component of gravity in the x-direction
E = Young's modulus of the cupular membrane material
ν = Poisson's Ratio of the cupular membrane material
R = ρ_f/ρ_0

$\epsilon = \frac{1}{2}\left(\frac{E}{1+\nu}\right)\frac{b^2}{\mu^2}\rho_0$

$\bar{g}_x = \left[\frac{b^2\rho_0}{\mu V}\right] g_x$ = nondimensional gravity

$\bar{\delta} = \left[\frac{\mu}{V\rho_0 b^2}\right]\delta$ = nondimensional displacement

V = some characteristic velocity in the problem

$\bar{V}_s = V_s/V$ = nondimensional skull velocity

$\bar{u} = u/V$ = nondimensional fluid velocity

$\bar{v} = v/V$ = nondimensional fluid membrane velocity

$\bar{w} = w/V$ = nondimensional cupular membrane velocity

$\bar{y} = y/b$ = nondimensional depth coordinate

$\bar{t} = \left[\frac{\mu}{\rho_0 b^2}\right] t$ = nondimensional time

b = thickness of the otoconial membrane

c = thickness of the cupular membrane

Δt = discrete time step increment

Δy = discrete spatial step increment